Neutronics analysis of a subcritical blanket system driven by a gas dynamic trap-based fusion neutron source for ^{99}Mo production

Hou-Hua Xiong[1,†], Qiu-Sun Zeng[2,†], Yun-Cheng Han[2,1], Lei Ren[2], Isaac Kwasi.Baidoo[3], Ni-Chen[4], Zheng-Kui zeng[1], Xiao-Yu Wang[1,2]

This study was supported by Anhui Provincial Key R&D Program (202104g0102007), Hefei Municipal Natural Science Foundation (2022011), and International Partnership Program of Chinese Academy of Sciences (116134KYSB20200001)
Correspondence: yuncheng_han@163.com (Yun-Cheng Han)
[1] School of Nuclear Technology and Chemistry & Biology and Hubei Key Laboratory of Radiation Chemistry and Functional Materials, Hubei University of Science and Technology, Xianning 437100, China
[2] Institute of Nuclear Energy Safety Technology, Hefei Institutes of Physical Science, Chinese Academy of Sciences, Hefei, Anhui, 230031, China
[3] Nuclear Reactors Research Centre, National Nuclear Research Institute, Ghana Atomic Energy Commission, Box LG 80, Legon-Accra, Ghana
[4] Teaching and Research Section of Nuclear Medicine, School of Basic Medical Sciences, Hefei Institutes of Physical Science, Anhui Medical University, Hefei, Anhui, 230031, China
† Both the authors equally contributed to this study.

Abstract:

Gamma-emitting radionuclide ^{99m}Tc is globally used for the diagnosis of various pathological conditions owing to its ideal single-photon emission computed tomography (SPECT) characteristics. However, the short half-life of ^{99m}Tc ($T_{1/2}$ = 6h) makes it difficult to store or transport. Thus, the production of ^{99m}Tc is tied to its parent radionuclide ^{99}Mo ($T_{1/2}$ = 66h). The major production paths are based on accelerators and research reactors. The reactor process presents the potential for nuclear proliferation owing to its use of highly enriched U (HEU). Accelerator-based methods tend to use deuterium-tritium (D-T) neutron sources but are hindered by the high cost of tritium and its challenging operation. In this study, a new ^{99}Mo production design was developed based on a deuterium-deuterium (D-D) gas dynamic trap fusion neutron source (GDT-FNS) and a subcritical blanket system (SBS) assembly with a low-enriched U (LEU) solution. GDT-FNS can provide a relatively high neutron intensity, which is one of the advantages of ^{99}Mo production. We provide a Monte Carlo-based neutronics analysis covering the calculation of the subcritical multiplication factor (k_s) of the SBS, optimization design for the reflector, shielding layer, and ^{99}Mo production capacity. Other calculations, including the neutron flux and nuclear heating distributions, are also provided for an overall evaluation of the production system. The results demonstrated that the SBS meets the nuclear critical safety design requirement (k_s<0.97) and maintained a high ^{99}Mo production capacity. The proposed system can generate approximately 157 Ci ^{99}Mo for a stable 24 h operation with a neutron intensity of 1×10^{14} n/s, which can meet 50% of China's demand in 2025.

Key words: Gas dynamic trap, Fusion neutron source, Molybdenum-99, Low-enriched uranium, Subcritical blanket system

1. Introduction

According to the World Nuclear Energy Association (WNA) [1], over 10000 hospitals worldwide use radioisotopes for the diagnosis and treatment of diseases. It is estimated that approximately 90% of radioisotopes are used in diagnostic procedures, among which ^{99m}Tc is the most commonly used, which benefits from its ideal characteristics of single-photon emission computed tomography (SPECT). Further analysis also demonstrates that the use of ^{99m}Tc constitutes

approximately 80% of nuclear medicine procedures, while 85% are used for diagnostic scans (Updated April 2022) [1]. However, the production of ^{99m}Tc ($T_{1/2}$ = 6 h) is tied to its mother radionuclide ^{99}Mo ($T_{1/2}$ = 66 h), which makes the study of ^{99}Mo production an essential research topic.

The production of ^{99m}Tc consists of two steps: 1) production of ^{99}Mo via mechanisms indicated in the schematic diagram of Fig. 1 (neutron-fission, gamma-fission, neutron-gamma, gamma-neutron, etc.) and 2) separation of ^{99m}Tc after it decays from ^{99}Mo through the emission of beta particles [2]. As indicated, ^{99}Mo and ^{99m}Tc have short half-lives. Nonetheless, unlike the relatively short half-life of ^{99m}Tc ($T_{1/2}$ = 6 h), which is the main hindrance for its transport, the half-life of ^{99}Mo ($T_{1/2}$ = 66 h) allows a relatively adequate time for transportation. Based on the half-life and transport time, the kinetics of producing ^{99m}Tc depend on the production of ^{99}Mo; that is, under normal circumstances, the resulting product ^{99}Mo is transported to the target country immediately after production, and subsequently its decayed product (^{99m}Tc) is quickly extracted and used in hospitals or nuclear medical centers.

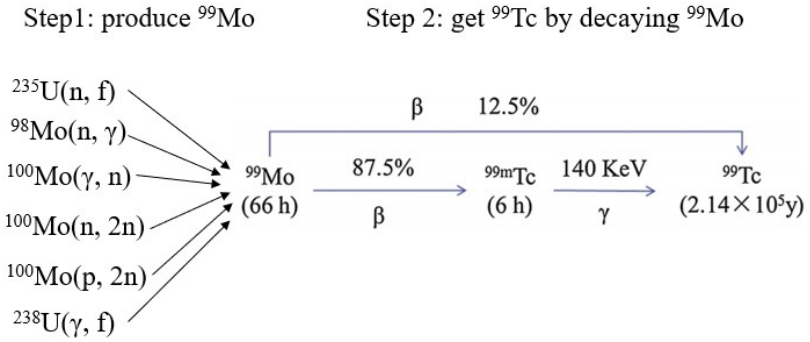

Fig. 1 Schematic diagram of the ^{99m}Tc production process

The global shortage of ^{99}Mo has recently been mainly attributed to aging nuclear reactors and their decommissioning [3-5]. A typical example is the event of the National Research Universal (NRU) in Canada, which produced approximately 40% of the world's ^{99}Mo supply but ceased production by October 31st, 2016 [3]. Currently, most ^{99}Mo isotopes are produced by the fission process with highly enriched U (HEU) reactors. These nuclear reactors are the Belgian Reactor 2 (BR-2), High Flux Reactor (HFR) in the Netherlands, LVR-15 Reactor in the Czech Republic, Maria Research Reactor (Maria) in Poland, Open Pool Australian Light Water Reactor (OPAL), and South African Fundamental Atomic Research Installation (Safari-1) [6]. Additional information regarding ^{99}Mo production, specific reactors, and target materials are listed in Table 1. Most of these reactors are not only facing the problems of aging and decommissioning, but also pose great risks of nuclear proliferation.

Table 1 Main ^{99}Mo production reactors[6]

Country	Reactor	Targets	Capacity*	Start	Est. stop
Belgium	BR-2	HEU	6500	1961	2026
Netherlands	HFR	LEU**	6200	1961	2022
Australia	OPAL	LEU	3500	2006	2030
Czech Republic	LVR-15	HEU	3000	1989	2028
South Africa	Safari-1	LEU	3000	1965	2025
Poland	Maria	LEU	2200	1974	2030
Russia	RIAR: three	HEU	890	1961-70	

USA	MURR	HEU	750	1966	
Argentina	RA-3	LEU	400	1967	2027
Total			26,440		

* 6-day Ci ^{99}Mo: a 6-day Ci is the measurement of the remaining radioactivity of ^{99}Mo six days after it leaves the processing facility (end of processing (EOP))

** In March 2021 HFR started using LEU for the production of radioisotopes.

To solve the problems of ^{99}Mo shortage and the nuclear proliferation of HEU targets, scientists have proposed a series of new methods to replace the path of HEU fission to produce ^{99}Mo. These methods can be divided into three categories: 1) ^{235}U(n, f)^{99}Mo reaction in low-enriched U (LEU) reactors [7, 8]; 2) solid target irradiation based on an accelerator, such as the neutron capture ^{98}Mo(n, γ)^{99}Mo reaction [9-13], ^{100}Mo(n, 2n)^{99}Mo reaction [14,15], ^{100}Mo(p, 2n)^{99}Mo reaction [16], ^{100}Mo(γ, n)^{99}Mo reaction [17], and photon-induced reaction of ^{238}U fission ^{238}U(γ, f)^{99}Mo [18]; and 3) LEU solution fission of the ^{235}U(n, f)^{99}Mo reaction in subcritical systems [19-23]. Among these, the last method is the most efficient and reliable means of production and has become a prime choice for ^{99}Mo production owing to the following advantages:1) compared to the solid target irradiation method based on an accelerator, the LEU solution can be effectively recovered and reused, thus significantly reducing the generation of radioactive waste; 2) the LEU fission method has a high production efficiency and low cost; and 3) comparing the LEU solution in subcortical systems to the HEU fission method, there is an advantage of avoiding nuclear critical safety accidents, and it also prevents nuclear proliferation. It is also relatively easy to apply for a license for construction and operation.

In 2021, Han et al. [22, 23] proposed a subcritical ^{99}Mo production system driven by an accelerator-based D-T neutron source, in which the accelerated deuterium ions bombard the tritium target, and the deuterium-tritium (D-T) fusion reaction generates neutrons. The LEU solution target is then irradiated by neutrons for the fission of ^{235}U via the ^{235}U(n, f)^{99}Mo reaction. Although this method does not require a supply of HEU, it has the disadvantage of using tritium. In addition to its high cost, it is difficult to obtain licenses for owning and operating tritium.

In this study, we propose a new design for ^{99}Mo production based on the LEU subcritical blanket system (SBS). The system is driven by a gas dynamic trap-based fusion neutron source (GDT-FNS). However, instead of the normal deuterium-tritium fusion reaction, a deuterium-deuterium (D-D) fusion reaction neutron is used to induce fission in ^{235}U. In addition to the apparent advantage of avoiding the HEU system, our proposed ^{99}Mo production system has numerous advantages, such as a compact structure, high neutron source intensity, and lack of tritium consumption, leading to low capital costs. To ensure the design safety and process optimization for the SBS ^{99}Mo production path, a neutronics analysis of the production system was performed using the SuperMC code (Monte Carlo Particle Transport code). A detailed neutronics analysis is provided for an overall evaluation of the production system, including the analysis of the subcritical multiplication factor (k_s), neutron flux, and heat deposition. A set of optimization parameters of the production system was obtained by maintaining a relatively high production rate and safety standard, including the geometric size, material components, and concentration of the LEU solution.

2 Model and Method

The LEU solution SBS driven by GDT-FNS mainly includes GDT-FNS and a ^{99}Mo SBS, as

shown in the schematic diagram in Fig. 2. The SBS is arranged in the high neutron flux region of the GDT, forming a fan-shaped blanket structure. Detailed descriptions are provided in sections 2.1 and 2.2.

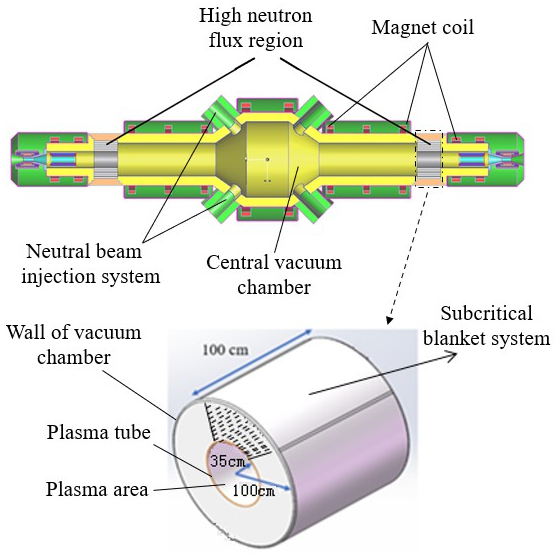

Fig. 2 Schematic diagram of the LEU solution SBS driven by GDT-FNS

2.1 Gas Dynamic Trap-based Fusion Neutron Source (GDT-FNS)

A GDT is a type of axisymmetric magnetic mirror device [24, 25]. Under the action of a specific magnetic field, the warm plasma constrained in the GDT vacuum chamber frequently collides and causes a fusion reaction, which can provide D-D or D-T fusion neutron sources, and the neutrons are "high at both ends and low in the middle." This type of neutron source has the advantages of a high neutron flux, large testing space, compact structure, and low construction cost. The GDT-FNS not only meets the performance of fusion materials/components, but its resulting high neutron flux can be used to conduct the study of applied nuclear technology, such as medical isotope production, neutron photography, neutron irradiation (breeding), and for the low-dose neutron effect in cells.

In this study, the GDT-FNS designed by the Hefei Institute of Physical Science [26, 27] was used to analyze the neutronics of a solution-based-LEU SBS. Quasi-monoenergetic neutrons with an energy of approximately 2.5 MeV were generated by means of the D-D () reaction in the central vacuum system (CVS). As indicated in Fig. 2, a GDT-FNS mainly includes a neutral beam injection system (NBI), CVS, magnetic coil (MC), and a high neutron flux region. The main parameters of the GDT-FNS with the D-D operation are listed in Table 2. Owing to the axisymmetric characteristics of GDT-FNS, SBSs with flexible settings can be arranged in the high neutron flux region to meet the increasing demand of ^{99}Mo production.

Table 2 Main parameters of GDT-FNS with D-D operation

Parameters	Value
Total length of GDT-FNS	2000 cm
Length of high neutron flux region	100 cm
Plasma tube radius at high neutron flux region	35 cm
Vacuum vessel radius at high neutron flux region	100 cm

Magnetic field in center	0.76 (0.94*) T
Magnetic field in plug	25.8 T
NBI power	50 MW
NBI angle	45 degree
NBI energy	70 keV
Gas feed rate	4200 eq.A
Peak fast ion density	7×10^{19} m^{-3}
Bulk plasma density	5×10^{19} m^{-3}
Electron temperature	1150 eV
Bulk ion temperature	2340 eV
Total neutron intensity of GDT-FNS	9.04×10^{15} n/s
Neutron intensity of high neutron flux region	8.54×10^{14} n/s

* At the start of discharge when the plasma beta is near zero.

The plasma parameters of the GDT-FNS system were simulated using the 1-D code DOL [28], which is based on a nonstationary numerical model describing the confinement of two different plasma components. During the simulations, a pure deuterium beam was injected into the central vacuum chamber, and the axial distributions of the D-D neutron generation rate were obtained, as shown in Fig. 3. The results demonstrate two high neutron flux regions, which are between the −700–−600 cm and 600–700 cm axial positions of the GDT-FNS. This important finding is the main reason for arranging the SBS in the high neutron flux region.

Fig. 3 The axial distribution of the D-D neutron generation rate of GDT-FNS

2.2 Subcritical Blanket System (SBS)

The SBS for the production of ^{99}Mo is arranged in the high neutron flux region of the GDT-FNS and forms a fan-shaped blanket structure. The main material components of the SBS include the LEU solution, solution container, reflector, and shielding layer. A schematic of the SBS ^{99}Mo production model is shown in Fig. 4. Based on the preliminary analysis and considering the FNS design constraints, certain geometrical and material parameters were fixed, such as the dimensions and specific material composition. The SBS was 100 cm long and less than 100 cm thick. The thickness of the LEU solution ranged between 30–50 cm, and the solid angle of the LEU solution relative to the central axis of the neutron source was between π/4-π/3. Thus, the variable parameters that need to be optimized for this study include the thicknesses of the LEU solution, reflector, and shielding, and the material types for the reflector and shielding layer. Considering the LEU solution, the UO_2SO_4 solution was selected with varying U concentrations (60 g/L to 150 g/L), with a ^{235}U enrichment of 19.75%. The low margin (60 g/L) was selected to obtain a considerable output of ^{99}Mo, and the upper limit (150 g/L) was based on the saturated U (UO_2SO_4) concentration at room temperature.

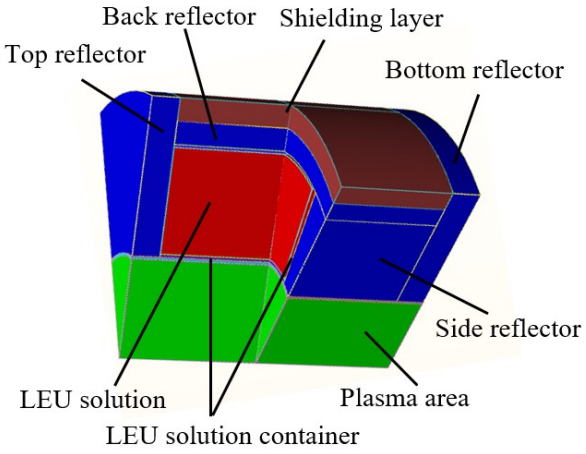

Fig. 4 Schematic structure diagram of SBS

2.4 Calculation Method

2.4.1 Calculation program and uncertainty

The neutronics parameters of the SBS were calculated using the Super Monte Carlo Simulation Program (SuperMC) version 3.2 [29] coupled with ENDF-VII cross-section libraries. Herein, the steady-state neutronics parameters of the SBS mainly included the k_s, neutron energy spectrum, activity of the produced ^{99}Mo, and heat deposition. In this study, 10 million statistical particles were used for each neutronics calculation, and the corresponding statistical uncertainties were less than 1%, except for the calculations of the energy deposition, where the statistical uncertainties were less than 3%.

2.4.2 Subcritical multiplication factor

The critical safety state of a subcritical system can be characterized by the k_s when the U fission system has an externally driven neutron source. Parameter k_s is defined as the ratio of the fission neutron number to the total neutron number in the system [30,31], as shown in equation (1).

(1)

Here, is the intensity of the externally driven neutron source [n/s], is the fission reaction rate [fission/s], and is the average number of neutrons generated by a fission reaction. The parameter k_s is usually required to be less than 0.98 to ensure the operational safety of a subcritical system [32-36]. The calculation of k_s was performed with a general source card (SDEF), where the energy spectrum was obtained from the first wall of the high neutron flux region of the GDT-FNS. The first wall neutron energy spectrum served as the external driver neutron source.

2.4.3 Activity and specific activity of produced ^{99}Mo

To evaluate the efficiency of the ^{99}Mo production and usage rate of U, we defined the total activity of ^{99}Mo produced by the SBS in one day (24 h operation) as A [Ci/day], and the daily ^{99}Mo produced per unit mass of ^{235}U as the specific activity (SA) [Ci/kg/day]. The amount of produced ^{99}Mo is increased by ^{235}U fission and reduced by its own decay. Thus, the number of ^{99}Mo nuclides [N(t)] at time t [s] changes according to equation (2) as follows:

(2)

where is the number of ^{99}Mo nuclides at time t [s], λ is the decay constant of ^{99}Mo, is the fission yield of ^{99}Mo (0.061), Σ is the macroscopic fission cross-section of ^{235}U [barns], and Φ is the neutron flux [$cm^{-2}s^{-1}$].

By defining and integrating equation (2), an activity equation (3) is obtained, which is consistent with the generalized activity equation[37].

(3)

However, in an SBS, the activity equation can be modified to obtain equation (4) as follows:

(4)

In this case, the neutron flux (Φ) is replaced with , that is, the external neutron source intensity [n/s] from the high neutron flux region of the GDT-FNS. Σ is equal to , where [barns] is the average microscopic fission cross-section of a ^{235}U atom. is the total number of ^{235}U atoms in the SBS, which is equal to , where is the Avogadro constant (6.02×10^{23}), M is the relative atomic mass of ^{235}U equal to 235, and m is the mass of ^{235}U[g] in the LEU solution

In this study, was calculated by setting the tally 4 card and multiplier card FM4 in the input file. Therefore, by substituting the values into equation (4), the daily production of ^{99}Mo in SBS can be evaluated.

2.4.4 Neutron and gamma flux calculation

The neutron and gamma flux can be calculated with a tally 4 [38] card by setting the different particle types [Neutron (N) or Photon (P)] using equation (5):

(, (5)

where is the neutron or gamma flux of the point detector [particles/cm^2], (,,E,t) is the angular flux [particles/(cm^3/sh/MeV/rad)], is the position vector [cm], E is the energy of the incident particle [MeV], is the direction vector, and is time [sh;1sh = 10^{-8}s]. To evaluate the neutron flux distribution of the SBS, the heterogeneous coefficient K_H is introduced. This is defined as the ratio of the maximum value of the core thermal neutron flux to the average value. K_H is generally required to be less than 1.4 in a design [39].

2.4.5 Nuclear heat deposition

The nuclear heat deposition was calculated using a tally 6 card (T6) combined with a superimposed mesh tally card (FMESH). The calculation result for T6 is the average energy deposition on the calculated cell, as shown in equation (6) [38].

(6)

where is the total energy deposition in the cell [MeV/g], is the atom density (10^{24}. atoms/cm^3), m is the cell mass [g], is the microscopic total cross section [barns], and H(E) is the heating number [MeV/collision].

3 Results and Discussion

3.1 Neutron Spectrum of the High Neutron Flux Region of GDT-FNS

The neutron spectrum is a significant parameter of GD-FNS, which can affect the fission reaction efficiency. In this study, the neutron generation rate (Fig. 3) was used as the input data to calculate the neutron spectrum. The neutron spectrum of the plasma tube in the high-neutron-generation-rate region was obtained using the SuperMC program. The statistical error of the calculated neutron spectrum was ensured to be less than 1%. The spectral distributions are shown in Fig. 5. The results demonstrated that neutrons with an energy of approximately 2.5 MeV had the highest proportion, which is owing to the D-D reaction producing neutrons with an average energy of 2.5 MeV. In the subsequent neutronics design of the SBS, the calculated neutron spectrum is used as the external driver neutron source.

Fig. 5 Neutron spectrum in the high neutron flux region

3.2 Preliminary Design of the SBS

The ^{99}Mo production by the SBS aims to achieve 50% of China's projected ^{99}Mo demand by 2025. China's current ^{99}Mo heavily relies on imports, as demand continues to grow. China's demand for medical ^{99}Mo was estimated to be approximately 16000 6-day Ci in 2019 [40]. Considering an annual growth rate of 5% [5], the estimated ^{99}Mo demand in 2025 will be approximately 21500 6-day Ci (i.e., 59 6-day per day). Determining these estimates requires the consideration of the decay losses during the separation and purification of the generated ^{99}Mo. Approximately 80% of the originally produced ^{99}Mo is lost during the 6-day period. However, approximately 10% [41] of the ^{99}Mo cannot be extracted by chemical separation and purification processes. Therefore, the daily ^{99}Mo demand is estimated to be 298 Ci in 2025 and 447 Ci in 2035.

When determining the preliminary design of the SBS, the following constraints were considered: 1) To ensure the nuclear critical safety of the LEU solution SBS, k_s must be less than 0.98 [32-36]. However, considering the neutron source fluctuation and measurement uncertainty, as well as other uncertain factors, k_s was limited to less than 0.97 to provide sufficient critical safety margins. 2) The U concentration was limited to range between 60–150 g/L. The upper limit, as indicated in the earlier sections, is owing to the saturation of UO_2SO_4 at 150 g/L. 3) The *SA* should be as high as possible.

The initial conditions for the calculation models were set as follows: the inner diameter of the plasma tube was 35 cm, the inner and outer radii of the LEU solution were between 37–74 cm, the thickness of the LEU solution container wall was 1 cm, the solid angle of the LEU solution was between$\pi/4$–$\pi/3$, and the thickness of the top and bottom reflectors was 5 cm. The back reflector was composed of a Be material with a thickness of 8 cm. There was a shielding thickness of 8 cm for materials composed of W, B, and polyethylene (PE) (Mass ratio 4:3:3). Different parameters of k_s, *A*, and *SA*, were calculated by changing the U concentration and solid angle. The corresponding calculation results are listed in Table 3.

Table 3 Preliminary calculation results of the different SBS design parameters (cases 1–6)

Case	Solid angle/rad	U concentration /gL^{-1}	LEU volume/L	^{235}U mass/kg	k_s	A/Ci	SA/Cikg^{-1}
1	π/4	100	145.2	2.904	0.9465	92.5	31.9
2	π/4	105	145.2	3.049	0.9671	130	42.6
3	5π/18	95	161.3	3.065	0.9410	91.7	29.9
4	5π/18	100	161.3	3.226	0.9612	125	38.7
5	5π/18	105	155.5	3.266	0.9681	156	47.8
6	π/3	95	193.5	3.677	0.9576	143	38.9

Note: A is the daily ^{99}Mo production of one SBS; SA is the specific activity (daily ^{99}Mo production of 1 kg ^{235}U).

As shown in Table 4, the k_s of case 5 satisfies the critical safety condition (less than 0.97), and the A is 156 C*i*. This activity is close to the 50% medical ^{99}Mo demand for the projected Chinese market by 2025 (149 Ci). In addition, the SA of case 5 is the largest, indicating that the ^{235}U use is also the most efficient compared to the other cases. Based on the results in Table 4, case 5 was selected as the preliminary scheme for the subsequent optimization design, including optimizing the U concentration, and the material types and sizes of the reflector and shielding.

3.3 The Impact of Uranium Concentration on the SBS

To study the influence of various U concentrations on the performance of the SBS ^{99}Mo production, the conditions of case 5 shown in Table 4 were selected for the detailed calculations with varying U concentrations. The volume of the LEU solution was set at 155.5 L, while the ^{235}U enrichment was fixed at 19.75%. The distribution of the varying U concentrations, the corresponding changes in the neutron multiplication factor k_s, and the daily ^{99}Mo production A are shown in Fig. 6.

Fig. 6 The impact of varying the U concentration (enrichment of 19.75% and solution volume of 155.5 L) on the distribution of k_s and A

Based on the results shown in Fig. 6, there is a general increasing dependence of both k_s and A on the increasing U concentration. In particular, the following can be deduced:1) As expected, the value of k_s demonstrates a strong dependence on the U concentration because it sharply increases as the U concentration increases. However, note that at a U concentration of 110 g/L, the k_s exceeds the design safety limit of 0.97. 2) Conversely, while the daily ^{99}Mo production A increases gently with an increasing U concentration, there is a sharp increase when the U concentration is above 90 g/L. 3) The most favorable condition in terms of the design nuclear critical safety is when the U concentration is just below 105 g/L, where k_s is less than 0.97. Therefore, the U concentration was set to 105 g/L in the final design model.

3.4 Optimal Design of Reflector

The reflector is arranged on the outside of the LEU solution and can reflect the neutrons back into the U solution to minimize neutron leakage and improve the use of neutrons. The selection of the reflector material and size has an important influence on the efficiency of the ^{99}Mo production and its associated k_s. The commonly used reflectors are Be metal, BeO, graphite (GR), heavy water

(D_2H), zirconia (ZrO_2), among others. In this section, case 5 is adopted for the calculation, and the thickness of the back reflector is set to 8 cm, while the other parameters remain unchanged. The values of k_s were calculated by changing the reflector materials, the results of which are shown in Fig. 7.

Fig. 7 Variations in k_s using different reflector materials

The k_s values obtained using different reflector materials demonstrate a maximum value for the case of Be as a reflector, which indicates that Be presents the best reflector effect for the selected conditions. Therefore, Be was selected as the reflective material for the SBS design. The subsequent optimization (calculation) process for k_s and A was performed by changing the thickness of the Be reflector. The results are shown in Fig. 8.

Fig. 8 k_s and A values varying with the thickness of the Be reflector

The calculation results demonstrate that the values of k_s and A increase as the thickness of the Be reflector increases. This trend emphasizes the beneficial effect of neutron use in SBS, with a corresponding benefit to the ^{99}Mo production. In addition, the optimum thickness of the Be reflector is approximately 10 cm; beyond 10 cm, only a marginal increase in A is observed with a relatively significant increase in k_s. Thus, to benefit from the capital cost of the reflector material, minimizing the geometric dimension of the entire SBS while improving the critical safety, a reflector thickness of 10 cm was plausible.

3.5 Shielding Layer Optimization Design

A shielding layer was used to reduce the neutrons and gamma radiation in the environment. Different shielding materials have varying shielding abilities for neutrons and gamma-rays. Eight types of materials were selected for the shielding study to reasonably select the material and thickness of the shielding layer; eight types of materials were chosen for the shielding study. The eight types of materials were Fe, Pb, W, Fe/B (weight ratio 1:1), W/B (weight ratio 1:1), Fe/PE (weight ratio 1:1), W/PE (weight ratio 1:1), and W/B/PE (weight ratio 4:3:3). The shielding performances of the different materials were evaluated with a thickness of 8 cm. The corresponding k_s values and average neutron fluxes outside the shielding layer were calculated. The results and their distributions are shown in Fig. 9.

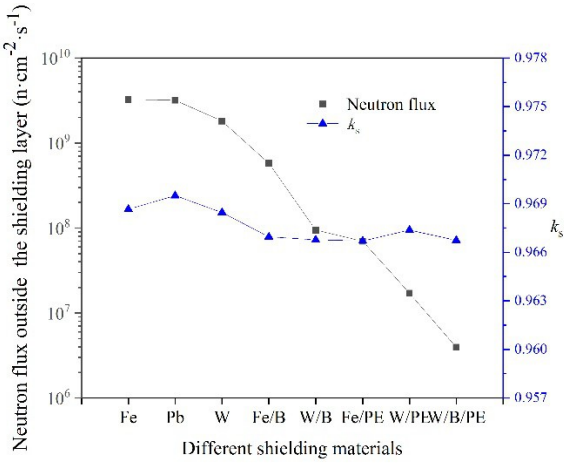

Fig. 9 Distributions of k_s and the average neutron flux (outside the shielding layer) varying with different shielding materials

The results demonstrate that the different shielding materials have little influence on the k_s value, that is, the difference between the maximum (0.9695) and minimum values (0.9667) is only 0.0028, as shown in Fig. 9. This indicates that W/B/PE had the best shielding effect for neutrons, which is expected because B has a very good thermal neutron absorption ability; PE is a good neutron moderator, while W, Fe, and Pb, have good gamma shielding. Overall, considering the shielding performance of the material against the neutrons and gamma rays and avoiding the toxic lead material, the composite material of W/B/PE was selected as the shielding material.

The influence of the varying W/B/PE thicknesses on k_s and the shielding performance were further studied. The calculation results are shown in Fig. 10, which demonstrate that k_s presents no significant change as the shielding thickness increases because the shielding material contains B, which absorbs neutrons. However, the average neutron flux and gamma flux outside the shielding layer decrease with an increase in the thickness of the shielding material.

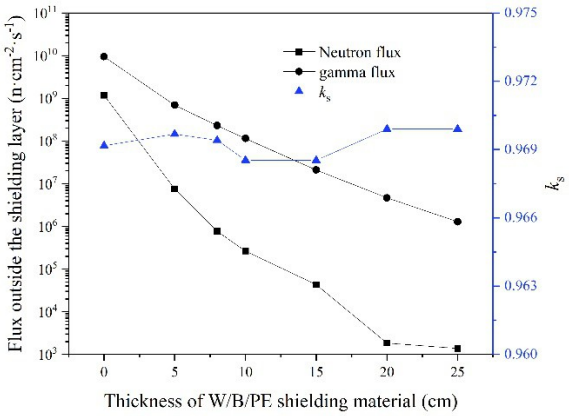

Fig. 10 The neutron flux and gamma flux outside the shielding layer and k_s varying with the thickness of the W/B/PE shielding material

According to the requirements of the shielding design, to limit the radiation impact from thermal neutron-activated products, the thermal neutron flux should be less than 1×10^5 cm^{-2}s^{-1}, and the gamma flux should be less than 4×10^{10} cm^{-2}s^{-1} [42, 43]. The results demonstrate that when the thickness of W/B/PE is 15 cm, the average neutron flux outside the shielding layer is 4.31×10^4

$cm^{-2}s^{-1}$, whereas the average gamma flux is 2.10×10^{7} $cm^{-2}s^{-1}$ with $k_s = 0.9685$. These values meet the requirements of shield design and nuclear critical safety margin.

3.6 Neutron Flux Distribution of SBS

The radial and axial neutron flux distributions of the SBS were calculated, the results of which are shown in Fig. 11 (a) and (b), respectively, demonstrating that the neutron flux in the U fission zone is of the order of 10^{11} n/cm^2·s (average of 3.73 $\times10^{11}$ n/cm^2. S; peak value of 4.94 $\times10^{11}$ n/cm^2·s). In addition, the neutron flux rapidly decreases after exiting the reflector layer (i.e., in the shielding layer). This sharp decrease confirms the effectiveness of the shielding materials indicated in the previous sections. In the axial direction, the neutron flux remains constant across the U solution, whereas the neutron flux at both ends of the reflector layer sharply decreases. The average neutron flux was calculated to be 3.88×10^{11}n/cm^{2}s and the maximum neutron flux was 4.72×10^{11}n/cm^{2}s. As defined in Section 2.4.4, K_H can be calculated as $4.72\times10^{11}/3.88\times10^{11} = 1.22$, which meets the design requirements (K_H needs to be less than 1.4). This demonstrates that the radial and axial neutron flux distributions in the SBS are relatively uniform, which is beneficial for the efficient use of ^{235}U and the safe operation of the system.

Fig. 11 (a) Radial neutron flux distribution of SBS; (b) axial neutron flux distribution of SBS

The neutron energy spectrum characteristics of the U solution layer, outer U container, reflector layer, and shielding layer were calculated as shown in Fig. 12. The results demonstrate that there are two thermal neutron peaks in the thermal neutron region (10^{-8}–10^{-6} MeV) and a fast neutron peak (approximately 2.5 MeV). The two thermal neutron peaks are owed to the H_2O in the U solution, which served as a neutron moderator. This moderation causes many neutrons to be moderated into thermal neutrons. The fast neutron peak appears because the external neutrons driving the SBS are mainly the 2.5 MeV neutrons (D-D reaction neutrons). In addition, fast neutrons were produced by the fission of ^{235}U.

Fig. 12 Neutron energy spectrum of the different components in SBS

3.7 Nuclear Heat Distribution of SBS

To obtain the distribution of the nuclear heat in each component of the SBS, a tally card (T6) combined with FMESH was used to calculate the nuclear heat deposition. The visualization function of the SuperMC code was used to display the results, as shown in Fig. 13 (a) and (b).

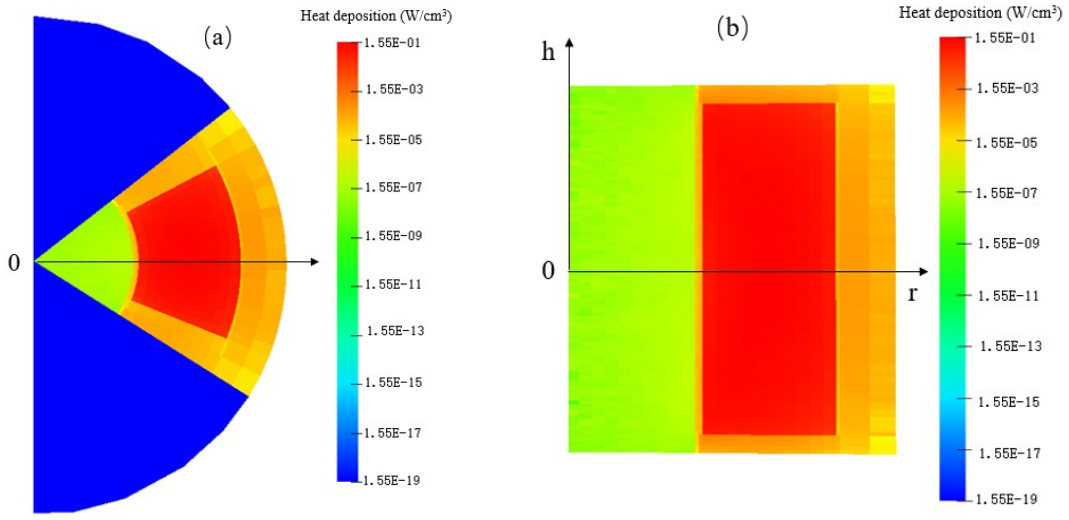

Fig. 13 (a) Nuclear heat distribution in the central radial section of SBS; (b) nuclear heat distribution in the central axial section of SBS

The results demonstrate that the nuclear heat is mainly deposited in the LEU solution, with a maximum nuclear heat of 1.53×10^{-1} W/cm^3 at the central position. The minimum nuclear heat was determined to be 4.57×10^{-3} W/cm^3 at the edge position. The average nuclear heat was 7.01×10^{-2} W/cm^3, and the total nuclear heat was 10.9 kW. The average nuclear heat in the reflector layer was found to be 1.21×10^{-4} W/cm^3, while the average nuclear heat in the shielding layer was 5.57×10^{-5} W/cm^3. The nuclear heats of the reflector and shielding layers were approximately 2–3 orders of magnitude lower than that of the LEU solution. This is because the nuclear heat mainly arises from the fission energy generated by the fission of ^{235}U, and the nuclear heat of the reflector and shielding layers is mainly from neutrons and gamma radiation energy deposition, which is significantly lower than the fission energy. COMSOL [44] was used to simulate the cooling system; according to the simulation results, the fuel solution may boil within 2 h if a cooling system is not added. The simulation results also demonstrate that a supplied inlet H_2O coolant temperature of 22 °C and flow velocity of 1.0 m/s will be sufficient to maintain the fuel solution temperature below 90 °C.

Based on the aforementioned analysis, the optimized design results for the ^{99}Mo production by SBS driven by GDT-FNS are listed in Table 4.

Table 4 Final optimized design and parameters of ^{99}Mo production SBS

Zone		Length (cm)	Thickness (cm)	Material
Plasma at SBS		90	35	D
Plasma tube		90	1	Fe
LEU solution		90	36	UO_2SO_4 aqueous solution，^{235}U enrichment: 19.75%，U concentration 105g/L
LEU solution container		90	1	Fe
Reflector	Back reflector	90	8	Be
	Top & bottom reflector	54	5	
	Side reflector	90	8	
Shielding layer		90	15	W/B/PE
Parameters		*Value*		

k_s	0.9685
SA	48 Ci/daykg
Yield of ^{99}Mo	157 Ci/day

4. Conclusions

In this study, an LEU SBS driven by GDT-FNS for ^{99}Mo production was proposed. A neutronics analysis of the ^{99}Mo production system was conducted using the Monte Carlo method (SuperMC code). The neutronics analysis includes the calculation of the neutron spectrum in the region of the high neutron generation rate of the GDT-FNS. The analysis also covers the preliminary design and optimization assessments related to different U concentrations and their ^{99}Mo production activities. Other analyses include the optimization design of the reflector and shielding layer, neutron flux, and the nuclear heat distribution of the SBS.

In all optimization cases, the designed system must meet the safety requirements and the amount of ^{99}Mo production necessary to meet 50% of China's projected ^{99}Mo demand in 2025. The preliminary assessment, as shown in case 5 in Table 4, demonstrated the most favorable conditions, where the U concentration was 105 g/L for an LEU solution of 155.5 volume/L with a mass of 3.266 kg and a subcritical multiplication factor of 0.9681. A further analysis was performed by placing the upper limit of the LEU solution volume at 155.5 and varying the mass of the LEU (19.75% enrichment) in the solution. The distribution was compared with the daily ^{99}Mo production and its impact on the subcritical multiplication factor. Based on this analysis, the most favorable condition in terms of the designed nuclear critical safety was a U concentration of 105 g/L for a k_s value near 0.97. Other analyses included shielding and reflector material selection and design optimization. Calculations demonstrated that Be (10 cm thick) and W/B/PE (15 cm thick) were suitable for serving as the reflector and shielding layers. The main optimized parameters are summarized as follows:

1) The optimal value for the subcritical multiplication factor (k_s) for the designed SBS was 0.9685, while the average neutron flux and gamma flux outside the shielding layer were found to be 4.31×10^4 n/cm^{2}s and 2.10×10^7 n/cm^{2}s, respectively. The distribution of the neutron flux and nuclear heating in the SBS were relatively uniform, as indicated by the K_H-value of 1.12, which further ensures the enhanced operational safety of the system.

2) The SBS allows for a high ^{235}U use, that is, 48 Ci ^{99}Mo can be produced from 1 kg of ^{235}U.

3) A total of 157 Ci ^{99}Mo can be produced by one SBS per day. Because the GDT-FNS is an axisymmetric structure and the solid angle of the SBS is only $5\pi/18$, multiple SBSs can be simultaneously arranged in the high neutron flux region of the GDT-FNS. According to the calculations, two and three of the SBSs designed in this study for the ^{99}Mo production can meet the demand of the Chinese market by 2025 and 2035, respectively.

The SBS driven by the GDT-FNS ^{99}Mo production system has the advantages of a high production efficiency, low nuclear waste, and low cost. Our study indicates that this system can be used as a potential facility for ^{99}Mo production. However, to make the system more feasible and practical, it is necessary to perform further detailed design studies, such as a U burnup analysis, ^{99}Mo separation, and purification technique verification.

Author contributions The conception and design were originally proposed by Yun-Cheng Han, to which all authors contributed. The material preparation, data collection, and analysis, were performed by Hou-hua Xiong,

Qiu-sun Zeng, and Yun-Cheng Han. The first draft of this manuscript was written by Hou-Hua Xiong. All authors have commented on all versions of the manuscript, and have read and approved the final manuscript.

References

1. World Nuclear Association. Radioisotopes in Medicine. https://www.world-nuclear.org/information-library/non-power-nuclear-applications/radioisotopes-research/radioisotopes-in-medicine.aspx
2. Z.W. Li, Y.C. Han, X.Y. Wang, et al., Production status and technical prospects of medical radioisotope ^{99}Mo/^{99m}Tc. Nucl. Phys. Rev. 36 (2019) 170–183, https://doi.org/10.11804/NuclPhysRev.36.02.170 (in Chinese)
3. L.M. Filzen, L.R. Ellingson, A.M. Paulsen, et al., Potential ways to address shortage situations of Mo-99/Tc-99m. J. Nucl. Med. Technol. 2017, 45(1). https://doi.org/10.2967/jnmt.116.185454
4. G.S. Thomas, J. Maddahi, The technetium shortage. J. Nucl. Cardiol. 17, 993–998 (2010). https://doi.org/10.1007/s12350-010-9281-8
5. Gould P, Medical isotope shortage reaches crisis level. Nature, 2009, 460(7253): 312-314. https://doi.org/10.1038/460312a
6. OECD-NEA. The Supply of Medical Isotopes: An Economic Diagnosis and Possible Solutions, OECD Publishing, Paris, 2019. https://doi.org/10.1787/9b326195-en.
7. R. Raposio, G. Thorogood, K. Czerwinski, et al., Development of LEU-based targets for radiopharmaceutical manufacturing: A review. Appl. Radiat. Isotopes. 2019, 148: 225-231. https://doi.org/10.1016/j.apradiso.2019.03.019Y.
8. L. Chen, R. Yan, X. Kang et al., Study on the production characteristics of ^{131}I and ^{90}Sr isotopes in a molten salt reactor. Nucl. Sci. Tech. 32, 33 (2021). https://doi.org/10.1007/s41365-021-00867-1
9. S. Hasan, M.A. Prelas, Molybdenum-99 production pathways and the sorbents for ^{99}Mo/^{99m}Tc generator systems using (n, γ) ^{99}Mo: a review. Sn. Appl. Sci. 2, 1782 (2020). https://doi.org/10.1007/s42452-020-03524-1
10. A. Qaaod, V. Ulik, ^{226}Ra irradiation to produce ^{225}Ac and ^{213}Bi in an accelerator-driven system reactor. Nucl. Sci. Tech. 31, 44 (2020). https://doi.org/10.1007/s41365-020-00753-2
11. A. Khorshidi, H. Ghafoori-Fard, M. Sadeghi, Epithermal neutron formation for boron neutron capture therapy by adiabatic resonance crossing concept. Int. J. Mod. Phys. E. 2014, 23(5), 1450032. https://doi.org/10.1142/s0218301314500323
12. M. Sadeghi, N. Hashemi, H. Afarideh, et al., Prediction of ^{94m}Tc production for positron emission tomography studies using the Monte Carlo code MCNPX-2.6[J]. Appl. Radiat. Isotopes. 2013, 82: 347-350. https://doi.org/10.1016/j.apradiso.2013.09.010
13. A. Khorshidi, M. Sadeghi, A. Pazirandeh, et al., Radioanalytical prediction of radiative capture in ^{99}Mo production via transmutation adiabatic resonance crossing by cyclotron. J. Radioanal. Nucl. Ch. 2014, 299(1), 303–310. https://doi.org/10.1007/s10967-013-2749-7
14. Y. Nagai, Y. Hatsukawa, Production of ^{99}Mo for nuclear medicine by ^{100}Mo (n, 2n) ^{99}Mo. J. Phys. Soc. Jpn. 2009, 78(3): 033201. https://doi.org/10.1143/JPSJ.78.033201
15. Capogni, M. Pietropaolo, A. Quintieri, Lina, etal, 14 MeV Neutrons for ^{99}Mo/^{99m}Tc Production: Experiments, Simulations and Perspectives.[J].Molecules (Basel, Switzerland),2018,Vol.23(8): 1872. https://doi.org/10.3390/molecules23081872
16. M. Sadeghi, T. Kakavand, M. Aref , et al., Targetry of MoO_3 on a copper substrate for the no-carrier-added ^{94m}Tc production via ^{94}Mo(p,n) ^{94m}Tc reaction. Nucl. Sci. Tech. 2009,20(01):22-26. https://doi.org/10.13538/j.1001-8042/nst.20.22-26.
17. V.N. Starovoitova, L. Tchelidze, D.P. Wells, Production of medical radioisotopes with linear accelerators. Appl. Radiat. Isotopes. 2014, 85: 39-44. https://doi.org/10.1016/j.apradiso.2013.11.122
18. M.A. Brown, Y. Karslyan, A.G. Servis, et al., Separation and purification of Mo-99 produced from natrral U_3O_8 targets via photo-fission. ANL. 2021. https://doi.org/10.2172/1838609
19. S. Chemerisov, A. J. Youker, A. Hebden, et al., Development of the mini-SHINE/MIPS experiments at ANL, Trans. Am. Nucl. Soc. 2012, 107(Nov.):74-77. (PDF) Development of the mini-SHINE/MIPS experiments at ANL (researchgate.net)
20. G. R. Piefer, K. M. Pitas, E. N. Van Abel, et al., Mo-99 production using a subcritical assembly. Paper presented at the 1st Annual Mo-99 Topical Meeting, La Fonda Hotel Santa Fe, New Mexico, December 4-7, 2011. S6-P3_Piefer-Paper.pdf (anl.gov)
21. L. Pardo, P. Daylen, P. Daniel et al., Coupled multi-physics simulation for the evaluation of an accelerator-driven aqueous homogeneous subcritical system for medical isotope production. Prog. Nucl. Energ. 134, 103–117 (2021). https://doi.org/10.1016/j.pnucene.2021.103692
22. L. Ren, Y.C. Han, J.C. Zhang, et al., Neutronics analysis of a stacked structure for a subcritical system with LEU solution driven by a DT neutron source for ^{99}Mo production. Nucl. Sci. Tech. 2021, 32(11): 1-11. https://doi.org/10.1038/504202a20

23. L. Ren , Z.W. Li , Y.C. Han , et al., Neutronics study of a subcritical system driven by external neutron source for ^{99}Mo production. Fusion Eng. Des. 2021, 165(1):112263. https://doi.org/10.1016/j.fusengdes.2021.112263
24. A.A. Ivanov, V.V. Prikhodko, Gasdynamic trap: an overview of the concept and experimental results. Plasma. Phys. Contr. F. 2013, 55(6): 063001. https://doi.org/10.1088/0741-3335/55/6/063001
25. A.A. Ivanov, V.V. Prikhodko, Gas dynamic trap: experimental results and future prospects. Phys-Usp+. 2017， 60 (5）： 509−533. https://doi.org/10.3367/UFNe.2016.09.037967
26. W.J. Yang, Q.S. Zeng, C. Chen, et al., Shielding design and neutronics calculation of the GDT based fusion neutron source ALIANCE. Fusion Eng. Des. 2021, 164: 112221. https://doi.org/10.1016/j.fusengdes.2020.112221.
27. Q.S. Zeng, D.H. Chen, M.H. Wang, High-field neutral beam injection for improving the Q of a gas dynamic trap-based fusion neutron source. Nucl. Fusion. 2017. 57(12): p. 126059. https://doi.org/10.1088/1741-4326/aa848c
28. D.V. Yurov, V.V. Prikhodko, Y.A. Tsidulko, Nonstationary model of an axisymmetric mirror trap with nonequilibrium plasma. Plasma Phys. Rep. 42 (2016) 210–225. https://doi.org/10.1134/S1063780X16030090
29. Y. WU, J. Song, H. Zheng, et al., CAD-Based Monte Carlo Program for Integrated Simulation of Nuclear System SuperMC. Ann. Nucl. Energy. 82, 161 (2015). https://doi.org/10.1016/j.anucene.2014.08.058
30. Q.F. Zhu, Y.Q. Shi, D.S. Hu, Research on Neutron Source Multiplicati on Method in Nuclear Critical Safety. Atomic Energy Sci. Technol. 2005 (02): 97-100. 10.3969/j.issn.1000-6931.2005.02.001 (in chinese)
31. M. Salvatores, Accelerator driven systems (ADS), physics principles and specificities. J. Phys. IV. 1999, 9(PR7): Pr7-17-Pr7-33. https://doi.org/10.1051/jp4:1999702
32. H.Y. Meng, Y.W. Yang, Z.L. Zhao, et al., Physical studies of minor actinide transmutation in the accelerator-driven subcritical system. Nucl. Sci. Tech. 2019,30(6). https:// doi.org/10.1007/s41365-019-0623-1
33. H. Nifenecker, S. David, J. M. Loiseaux, et al. Basics of accelerator driven subcritical reactors. Nucl. Instrum. Meth.A. 2001, 463(3): 428-467. https://doi.org/10.1016/s0168-9002(01)00160-7
34. R. Akkaya, E. Kemah, Tokgoz S R, Investigation of New Generation Accelerator Driven Subcritical Reactor System (ADS) in Nuclear Energy Production. App. Sci. Report. 2016, 13(3). https://doi.org/10.2139/ssrn.3201532
35. B. Ye, C.W. Yang,C.Z. Measurement of k eff by delayed neutron multiplication in subcritical systems. Nucl. Sci. Tech. 2018,29(2). https://doi.org/10.1007/s41365-018-0355-7
36. K.Q. Ruan, *Nuclear critical safety*. (Atomic Energy, Beijing, 2001) , pp.92-93 (in chinese)
37. A.J. Youker, S.D. Chemerisov, P. Tkac, et al., Fission Produced ^{99}Mo without a Nuclear Reactor. J. Nucl. Med. 2016:514. https://doi.org/10.2967/jnumed.116.181040
38. X-5 Monte Carlo Team. Briesmeister J F. MCNP-A General Monte Carlo N-Particle Transport Code, Version 5. Version 5, Los Alamos National Laboratory, 2003,10
39. Z.S. Xie, H.C. Wu, S.H. Zhang, *Physical Analysis of Nuclear Reactors*. (Atomic Energy, Beijing. 2003), pp.109-110 (in chinese)
40. China eight Department Association. *Medium and long term development plan for medical isotopes (2021-2035)*. 2021 (in chinese)
41. A.H.A. Sameh, Production cycle for large scale fission Mo-99 separation by the processing of irradiated LEU uranium silicide fuel element targets. Sci. Technol. Nucl. Ins. 2013(2013). https://doi.org/10.1155/2013/704846
42. Chinese industry standards, *Design criterion of radiation shield in the PWR nuclear power plant*.(NB/T 20194-2012.2012). (in chinese)
43. D.P. Li, Z.Q. Pan, *Radiation Protection Manual Volume III, Radiation Safety*. (Atomic Energy, Beijing, 1987), pp.270-271 (in chinese)
44. D. H. Daher, M. Kotb, A.M.Khalaf, et al., Simulation of a molten salt fast reactor using the COMSOL Multiphysics software. Nucl. Sci. Tech. 2020,Vol.31(12)